Faculty of Women for, Arts, Science, and Education

Scientific Publishing Unit

Journal of Scientific Research in Science

Basic Sciences

Volume 40, Issue 1, 2023

ISSN 2356-8372 (Online) \ ISSN 2356-8364 (print)

Journal of Scientific Research in Science 2023, 40, (1): 142-167

Contents lists available at EKB

Journal of Scientific Research in Science

Journal homepage: https://jsrs.journals.ekb.eg/

Egyptian Knowledge Bank
بنك المعرفة المصري

Scientific Publishing Unit

Water Pollution and its Treatment using nanocomposites of graphene oxide (GO 50%) / Zn2+ for different dyes and heavy metals using sol-gel synthesized

R. Atya[(a)*], N. Okasha[(a)], A.Azab[(b)], A.M. Baker[(c)]

(a) Faculty of Women for Arts, Science and Education, Ain Shams University, Cairo, Egypt.

(b) Solid State Physics Department, Physics Research Institute, National Research Centre, 33 El Bohouth St, Giza Dokki 12622, Egypt.

(c) Spectroscopy Department, Physics Research Institute, National Research Centre, 33 El Bohouth St., Dokki, P.O. 12622, Giza, Egypt.

Abstract:

In this study, Spinel nano ferrite (MFe_2O_4) ferrite powders were prepared by auto-combustion reaction. Nanoparticles have been synthesized by sol-gel method using citric acid as chemical catalyst while graphene Oxide prepared using Hammer technique and the starting raw materials as graphite powder. A straightforward procedure for creating magnetic nanoparticles coated with graphene oxide was disclosed (M = Zn. metal sites). Graphene oxide (GO) also causes the composite to have nanoparticles with a smaller dimensional size (3.61 nm). The structural identification of the samples was carried out using X-ray Diffraction (XRD), were used to characterize the structure of MFe_2O_4; the average crystallite size ranges from 26.7 to 35.1 nm. Transmission electron microscope (TEM), selected area electron diffraction (SAED) and IR spectra, which commonly had diameters between 25 and 120 nm. VSM was used to measure the magnetic characteristics coercivity (Hc) and saturation magnetization (Ms). Our samples are soft magnetic materials, as evidenced by the low coercivity of the magnetization curves. $ZnFe_2O_4$ nanoparticles and $ZnFe_2O_4$/GO 50% had saturation magnetizations (Ms) of 2.7902 and 1.4546 emu/g, respectively. According to the findings, MFe_2O_4 has a spinel-like structure with high porosity and surface area as well as significant saturation magnetization, making it a promising contender for a number of applications.

Keywords: Graphite, Graphene oxide, wastewater treatment, Nano ferrite, XRD, TEM, Magnetic nanomaterials, superparamagnetic.

***Corresponding author**: R. Atya, Physics Department, Faculty of Women for Arts, Science and Education, Ain Shams University, Cairo, Egypt.

E-mail: rehab.atya@women.asu.edu.eg

(Received 16 March 2023, revised 06 June 2023, accepted 12 June 2023)

https://doi.org/10.21608/JSRS.2023.200421.1104

1. Introduction

Water is sustenance of the life cycle. It needs to be looked after and protected from any pollution. It is essential for the health of both the human body and other living creatures, but it should never be contaminated. However, a result of human activity, water sources such rivers, wells, streams, and seas are contaminated. The natural water system on land is being contaminated by pesticides, industrial waste, urban rubbish, and other contaminants. The introduction of pollutants into an ecosystem, whether physical systems or living things, which causes instability, chaos, harm, or discomfort is referred to as pollution. Pollutants can be chemical substances or energy forms like sound, heat, or light. Pollutants, which make up pollution, can be either naturally occurring or imported materials or energies. When they are present more than normal levels when they are naturally occurring, they are regarded as pollutants.

The depletion of toxic dye wastewaters to the environment from industrial processes is a major environmental obstacle for water bodies. Organic dyes are one of the main groups of pollutants discharged into wastewater from the fabric, dyeing, and other industrial operations. The three groups of dyes are anionic, cationic, and non-ionic. The removal of anionic dyes, which are water soluble and produce exceptionally brilliant colors in water with acidic properties, is regarded to be the most challenging process [24]. Diverse separation techniques, including chemical, physical, and biological ones, are utilized to remove these wastewaters and a number of chemicals [25]. A promising area in the realm of water and wastewater treatment is the chemical pollutant removal employing magnetic nanoparticle as an adsorbent [1] $ZnFe_2O_4$ with cubic spinel structure has been widely used. Additionally, it has other beneficial characteristics like low cost, low toxicity, and high chemical stability [2].

Magnetic nano ferrites are significant Because they are used in so many different technological and varied domains. The magnetic nano ferrites have been used in a wide range of applications, such as magnetic refrigeration, magnetic storage, microwave absorbers, permanent magnets, magnetic ferrofluids, magnetic separation, switching, core, recording heads, magnetic shielding, and high frequency sensors.

Magnetic nanoparticles and their composites with sheet materials such as graphene oxide (GO) have received enhancing consideration as adsorbents for removal of dye from water sources due to the high surface area and large adsorption capacity [5]. The high specific surface area of graphene oxide GO ranges from 600 to 3500 m_2g^{-1}. The very hydrophilic functional groups on GO sheets are thought to be responsible for the material's dispensability [6]. A carbon-based nonmaterial called graphene oxide has shown intriguing adsorptive characteristics [59]. For dye adsorption, GO is widely employed [41].

Carbon atoms are arranged in a hexagonal lattice to form the structure of graphene oxide, a material with a one-atom thickness and special mechanical, optical, thermal, and electrical properties. [9, 10] At low energy limits, graphene oxide has an energy gap of zero so the electrons in graphene oxide satisfy an equation similar to Dirac's equation for particles of zero mass [11]. The molecular components of graphene oxide are carbon, hydrogen, and oxygen. Graphene is a two-dimensional, hexagonal-latticed crystal allotrope comprised entirely of carbon atoms. High optical transparency, excellent heat conductivity at normal temperature, and flexibility are only a few of its special qualities contained in a robust, nanoscale material.

Composite materials are created by combining two or more constituent materials that have distinctly different physical or chemical properties and that, on a macroscopic scale, remain separate and distinct inside the final structure. In recent years, graphene-based materials, such as ferrite/graphene composites, have emerged as innovative materials for several essential applications [25-28]. Particularly for energy storage. These composites might be excellent options for both battery systems and supercapacitors [14-18]. Additionally, the process of creating composite materials using carbon fibers, graphene, reduced graphene oxide, multiwall carbon nanotubes [19-21] etc. is promising for applications in electromagnetic shielding and wastewater treatment [12,13]and has a variety of potentials and environmentally acceptable uses [22-24].

The goal of this work is synthesis of nanocomposites from graphene oxide decorated with magnetic zinc ferrite nanoparticles to use in the treatment of various types of water pollution, such as dyes. Additionally, select the best nanocomposite that provides exceptional outcomes for eradicating water pollution and enhancing water efficiency.

2. Experimental and techniques:

2.1. Preparation of nano ferrites ($ZnFe_2O_4$) using the Sol- gel method

Due to their ease of solubility in water, the nitrates of the constituent ferrite metal ions—which are, the magnetic ceramics consisting of Fe^{3+} as the major constituent—are used as the reducing agent in the sol-gel method[30]of auto combustion, homogenous and highly reactive crystalline powders of stoichiometric amount of Metal Nitrate; MFe_2O_4; ($M= Zn^{+2}$),can be produced with reducing agent as Citric acid (CA) method ($C_8H_{12}O_7$) as (Reducing agent) which using as complete the reaction and stable the reaction, where the ratio of Zn to citric acid are Zn: Citric Acid = 1:x, then added aqueous solution to become liquid, to fixed the PH value up to 7 , put ammonia (NH_4) drop by drop then measure by PH. After that, using magnetic stirring, Mixed solution using Magnetic stirring at 80°C, which change to gel in color brownish viscous Gel. Finally, we obtain ferrites.

2.2. Synthesis of graphene oxide (GO)

Using the Hammerer method to prepare graphene oxide (GO) [29], through oxidation of graphite using sulfuric acid (H_2SO_4) and Graphite powders which mixing and continuous stirring by adding $NaNO_3$ Solution or $KMnO_4$ with stirring up temperature rise to 10°C, then put the Distilled water slowly up temperature rise to 98°C. Finally put H_2O_4 (Hydrogen peroxide) to form powder, by washed by HCL to remove the impurities and filters the powders by centrifuge to adjust PH ≤ 7. In the last dry the powder at 60°C for 24 h. We get Graphene Oxide (GO).

2.3. Synthesis of GO/M-Fe Composites by mechanical method [34-35]

The composite was fabricated from ferrite nanoparticles, MFe_2O_4 (M = Zn^{+2}), and graphene oxide using a. To make 1 g of the composite, $ZnFe_2O_4$/GO, we used 0.5 g of Go and 0.5 g of $ZnFe_2O_4$, and ball milling method we mixed them thoroughly. Next, we placed the composite in an ultrasonic tank for about 30 minutes to sonicate it. Finally, we used ball milling by adding specified quantities of solid MFGO to 200 ml of dye solutions with various beginning concentrations (100-12.5 mg/L), cationic dyes with varying initial concentrations (100-12.5 mg/L) were adsorb on the surface of magnetic nanoparticles made of MFe_2O_4/GO. After centrifuging 12.5 ml of dye solutions numerous times to remove the solid adsorbent, the flasks were swirled for 2.0 hours at room temperature (30°C) to identify the non-adsorbed dye by UV-vis spectrophotometry.

2.4. Material characterization

All TEM measurements were performed using a (HRTEM) [JEM-2100, with an operating voltage is 200 keV and gun type is Lab6 Emitter] was used to analyze the morphology of the prepared samples nanocomposite as a reference (HRTEM, Tokyo, Japan). XPERT-PRO-PANalytical -Netherland measurements the X-ray diffraction (XRD) in Nanotechnology Characterization center (NCC), Agriculture of Research center (ARC). CuK radiation with an absorbed wavelength (0.1542nm) and current of 30 mA was used to create an XRD pattern. the Physical Property: Measurement methods System's vibrating sample magnetometer (VSM), the samples' magnetic properties were examined at room temperature using a vibrating sample magnetometer (VSM; LakeShore -7410-USA)). The Raman spectroscopy was carried out using a Three samples were measured using FT-IR (Fourier transform infrared spectroscopy) Bruker- Model Vertex 80v with range between 400 and 4000 cm^{-1} [32].

3. Results and discussions

3.1. Structural analysis (XRD) of $ZnFe_2O_4$/GO nanocomposite:

The acquired typical patterns of the $ZnFe_2O_4$/xGO composite (x=0.50%) are shown in Fig (1). The synthesis of monophasic spinel $ZnFe_2O_4$ NPs, which are well known for ferrites, was confirmed by the observed diffraction peaks, ensuring the formation of the necessary ferrites in a single phase without any impurity's phases**.** The phases as (220), (311), (400), (422), (333), and (440) indicate the spinel cubic structure [31-33]. In addition, 111, 220, 311, 222, 400, 422, 511, 440 and 533 from the cubic system of zinc ferrite [34].

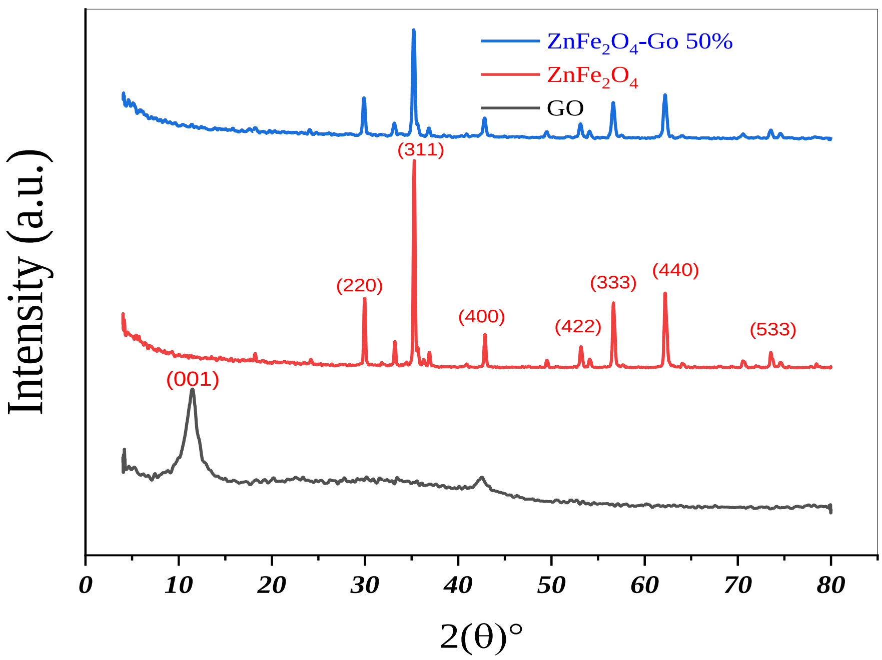

Fig (1): XRD patterns of the $ZnFe_2O_4$, $ZnFe_2O_4$ /GO 50% and GO

The average crystallite sizes of $ZnFe_2O_4$ and $ZnFe_2O_4$/GO 50% are 38.5and 26.7 nm using the Debye- Scherrer's formula: [35-37], are displayed in **Table1**

Table 1: XRD of $ZnFe_2O_4$ and $ZnFe_2O_4$/Go 50%, the crystallite size

Sample	FWHM (rad)	K	λ(nm)	D(nm)
$ZnFe_2O_4$	***0.00330014***	***0.94***	***0.154***	***46.02556603***
$ZnFe_2O_4$/Go 50%	***0.00567555***	***0.94***	***0.154***	***26.7593868***
GO	***0.040236309***	***0.94***	***0.154***	***3.616723041***

$$D_{hkl} = k\lambda / \beta \cos \theta \quad .... (1)$$

Where k is the crystalline phase factor (0.9), D_{hkl} is the average crystallite size (nm), 0.15406 nm is the X-ray wavelength, FWHM is the full width at half maximum, and is the Bragg's direction (in radians) at which the peak [311] is observed. From the Table, the average crystallite sizes range from 26.7 -38.5 nm. Moreover that, the sample of zinc ferrite displays the greatest average crystallite size. It suggests that it might be generated by a high-temperature exothermic reaction during the synthesis of the ferrite because it is well known that raising temperature during or after preparation accelerates the growth of the crystallites [36]. To analyze the morphology and particle size of products, the surface morphology and particle size of samples were looked at using FE-TEM. Photos of GO sheets fig (4a) (A and B) and $ZnFe_2O_4$/GO composites with 50% weighted graphene concentrations are shown in Fig (4 b) (C and D). According to the TEM micrograph, the uncoated sheets with stacking GO had a wrinkled paper-like texture. The identity $ZnFe_2O_4$ formed from the Zn^{2+} and Fe^{3+} ions anchored on the GO sheets eventually grew into nanospheres with diameter range of 120 and 25 nm.

3. 2. FTIR Study

Fig (2) depicts Carbonyl (C = O), aromatic (C = C), carboxyl (COOH), epoxy (C-O-C), and hydroxyl (O-H) groups are among the vibrational elements of the GO layer that form the FT-IR spectra of GO. The stretching vibrations of CH_2 bonds are shown by absorption peaks at 2926 cm^{-1} and 2850 cm^{-1}, respectively, whereas the carboxyl groups (O-H) produced by the water molecules are indicated by a prominent peak at 3200 cm^{-1}..[38] Ketone group (C=O) is responsible for the peak at 1627 cm^{-1}, while sp2 hybridization is responsible for the peak at 1544 cm^{-1}'s primary graphitic domain[39] (39). The C-O is visible in the band at 1457

cm^{-1}, and epoxy group C-O stretching is indicated at 1243 $cm^{-1.}$ Information regarding the C-O-C stretching of alkoxy groups can be found in the mode at 1020 cm^{-1}[40-42] The aromatic C-H distortion is responsible for the absorption peak at 803 cm^{-1} [41] .C-H bending vibrations cause spikes at 670, 594, and 461 cm^{-1}[42]. The FT-IR spectra of the GO-$ZnFe_2O_4$ nanocomposite showed a distinct peak corresponding to the Zn-O bond between 540 and 550 cm^{-1}. Intrinsic stretching vibrations are present in the first band, which is found at 540 cm^{-1} and belongs to the metal at the tetrahedral site (M-O), whereas the lowest band, which is observed at 420 cm^{-1} and belongs to the octahedral site, lacks these vibrations (M-O) [43].

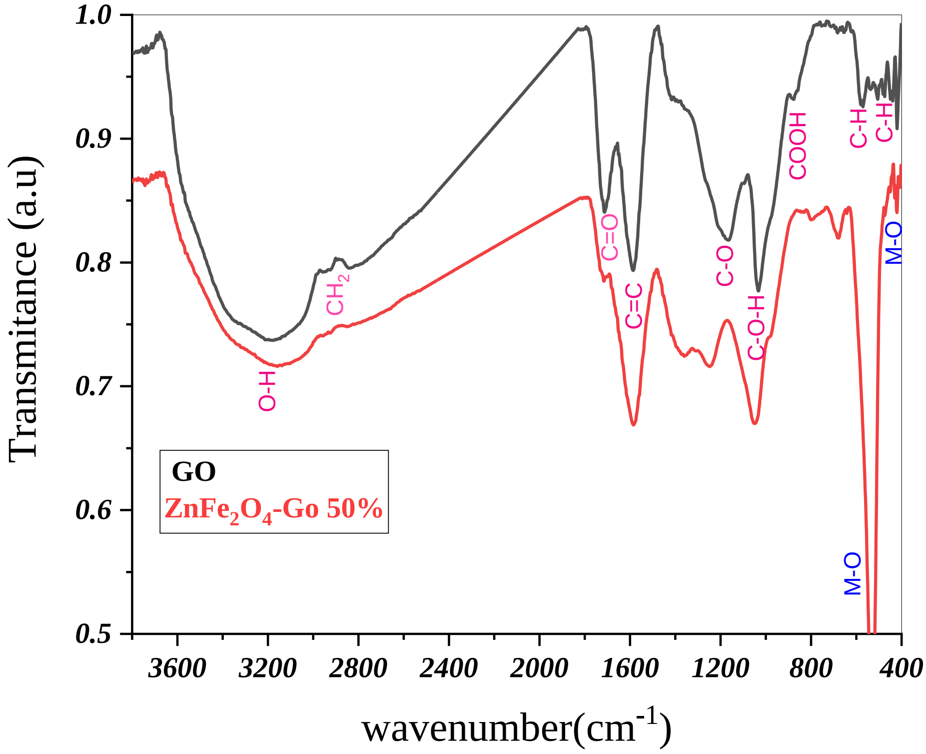

Fig (2): FTIR spectrum of the GO and $ZnFe_2O_4$-GO 50%

3. 3. Raman Spectrum

In Fig (3) the Raman spectrum of GO layer contains bands marked as D, G and 2D bands. The first-order D and G peaks, which result from sp_2 carbon's vibrations, were first observed at approximately 1346 cm^{-1} and 1597 cm^{-1}, respectively. The D-band displays crystalline material disorders and flaws linked to vacancies and grains [44]. As the thickness of GO varies, it is shown that the D peak's shape and location change. The optical E2g phonons in the Brillouin zone center, which are caused by The G peak is associated with the bond stretching of sp_2 carbon pairs in both rings and chains [45]. The quantity of flaws and oxygen atoms on the GO surface affect band D intensity [46-47]. Fig (3) illustrates the ID/IG ratio and the degree of disorder in this carbon-based substance. A well-known criterion for determining the size of the sp2 domain in a carbon structure with sp_3 and sp_2 links is the IG/ID ratio. According to estimates, GO's intensity ratio is 0.97. The Raman spectra of the composite $ZnFe_2O_4$/GO (50%) material were observed, and they exhibit both GO and $ZnFe_2O_4$ characteristics. The intensity ratio ID/IG was computed (0.98 -1.02). The $ZnFe_2O_4$ (spindle)-GO nano hybrid's ID/IG ratio (1.02) was larger than that of other pure and decorated GO, however, which was caused by the existence of additional defects brought on by interactions between the zinc ferrite and the graphene sheets.

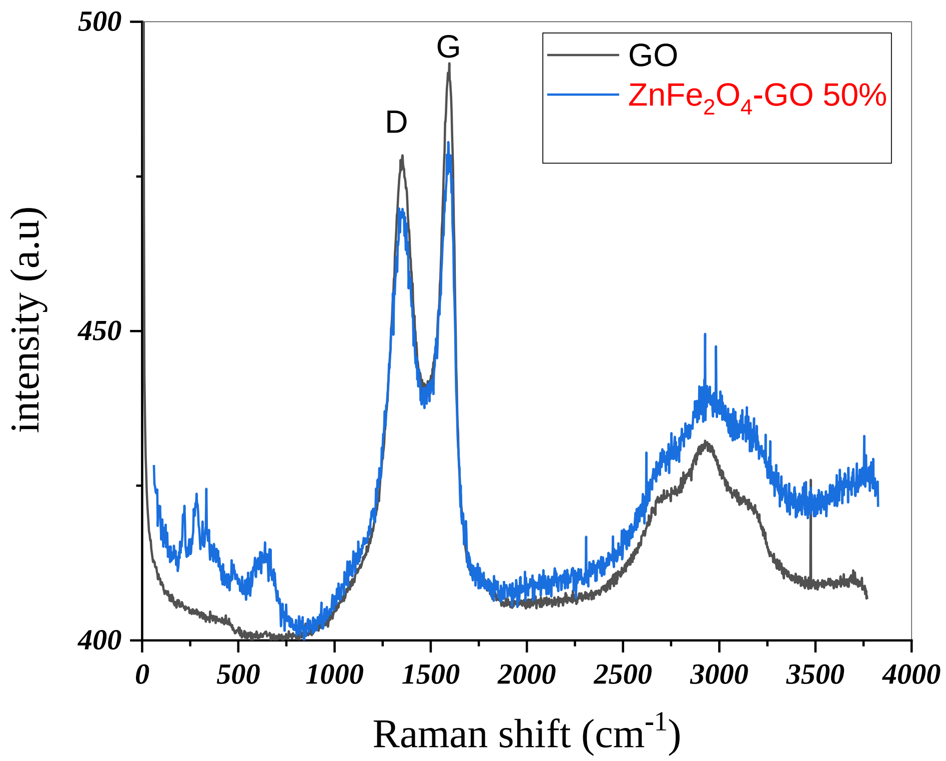

Fig (3): Raman spectrum of the GO, $ZnFe_2O_4$/GO 50%

3.4. Transmission electron microscopy (TEM) and microstructural characterization

The morphology and form of the investigated adsorbent materials, namely GO nanosheets and ZnF_2O_4/GO nanocomposites, were investigated using TEM techniques. Fig 4(a,b) illustrates how transparent the GO nanosheets were. In addition, wrinkles were seen, indicating that the GO sheets had a paper-like structure. The stacking of the ultrathin sheets with GO, It works as a nucleation site for nanostructure growth and supports the synthesis of Zinc ferrite by electrostatic contact. Its surfaces contain covalently linked oxygen-functional groups like epoxy, hydroxyl, and carboxyl groups. As the Zn^{2+} and Fe^{3+} ions anchored on the GO sheets self-assemble into $ZnFe_2O_4$, these nuclei expand into nanospheres with average diameters of 120 and 25 nm that are unmistakably conformed to Fig.4 (c,d)[47].

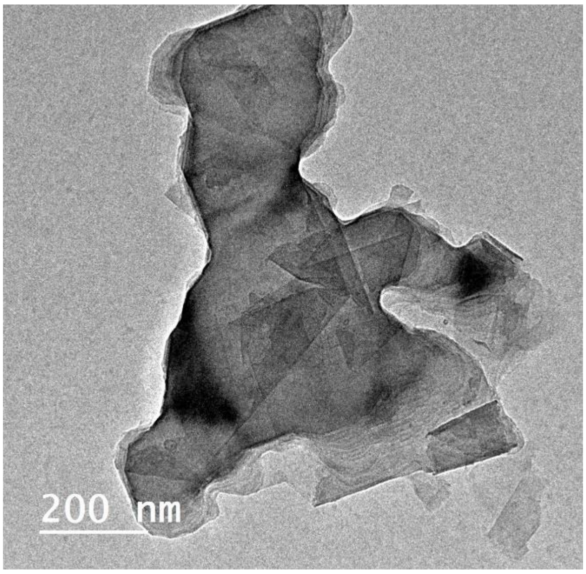

Image (A) o**f** Graphene oxide

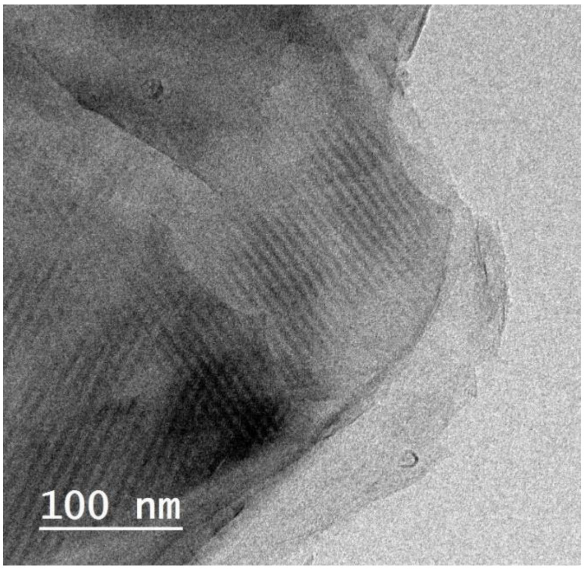

Image (B) of Go sheets

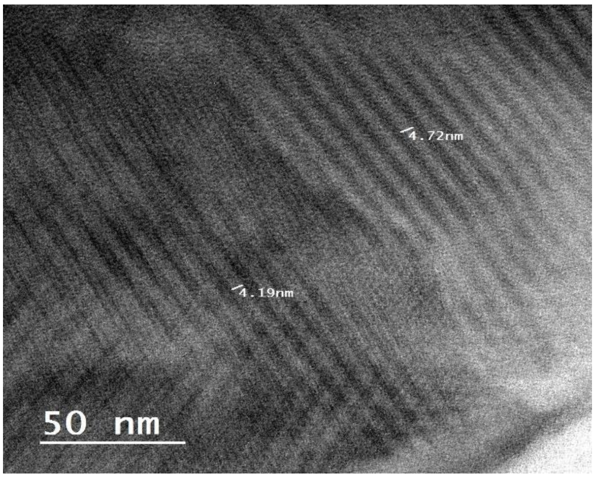

Image (C) of GO sheets

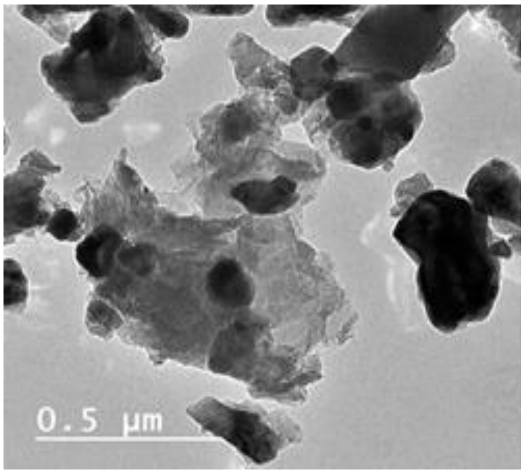

Image (D) **of** $ZnFe_2O_4$/GO 50%

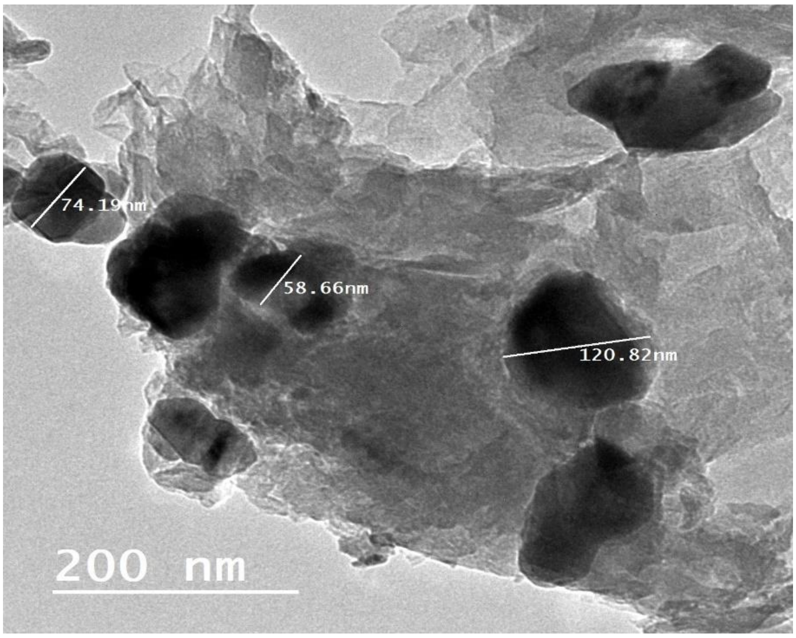

Image (E) of $ZnFe_2O_4$/GO 50%

Fig (4): TEM images of (A-C) GO sheets and $ZnFe_2O_4$/GO composites with (D and E) $ZnFe_2O_4$-GO 50 wt% graphene contents**.**

3. 5. Magnetic Properties

Using (VSM), the magnetic characteristics of the produced nano ferrites and ferrite/graphene composites were examined. Fig. (5) displays the plotted hysteresis loops. While the magnetization curves of $ZnFe_2O_4$ nanoparticles and $ZnFe_2O_4$/GO50% nanoparticles showed low coercivity (Hc), indicating the presence of small magnetic particles with paramagnetic properties in our soft material.[49]. It is possible to see paramagnetic materials responding to an applied magnetic field without any lingering magnetism after the magnetic field has been removed. A crucial characteristic for magnetic targeting carriers is this behavior [50]. It is well known that there are differences in particle size between ferromagnetism and superparamagnetic [48].

Table (2) The parameters of magnetization as M_s (saturation magnetization), H_C (Coercivity), and the Retentivity (M_r/M_s) for $ZnFe_2O_4$ and $ZnFe_2O$ / Go 50%.

Sample	Magnetization Ms (emu/g)	Coercivity (Hc) G	Retentivity (Mr) (emu/g)
$ZnFe_2O_4$	***2.7902***	***36.852***	***0.11712***
$ZnFe_2O_4$ / Go 50%	***1.4546***	***195.5***	***0.065631***

The $ZnFe_2O_4$ nanoparticles and $ZnFe_2O_4$/GO 50% had saturation magnetization values (Ms) of 2.7902 and 1.4546, respectively. Table 2 makes it evident that because the $ZnFe_2O_4$ NPs were wrapped in GO sheets, the Ms value of the GO-MFO sample was lower than that of the bare MFO NPs, The GO-MFO sample's Ms value was less than that of the plain MFO NPs. These numbers are powerful enough to produce an effective magnetic separation. The main influencing factor is the cation distribution between the two sublattice sites A and B, even though the saturation magnetization Ms is actually caused by a combination of many factors (intrinsic and extrinsic), including chemical composition, grain size, and A-site and B-site ion exchange interactions. The sum of the magnetization vectors at the two sublattices, or M_s=M_B-M_A, represents M_s as a vector quantity. The literature indicates that Fe^{3+} ions strongly prefer to occupy octahedral B-sites. However, Zn^{2+} ions can enter both A-sites and B-sites, though B-sites have larger ratios [51].

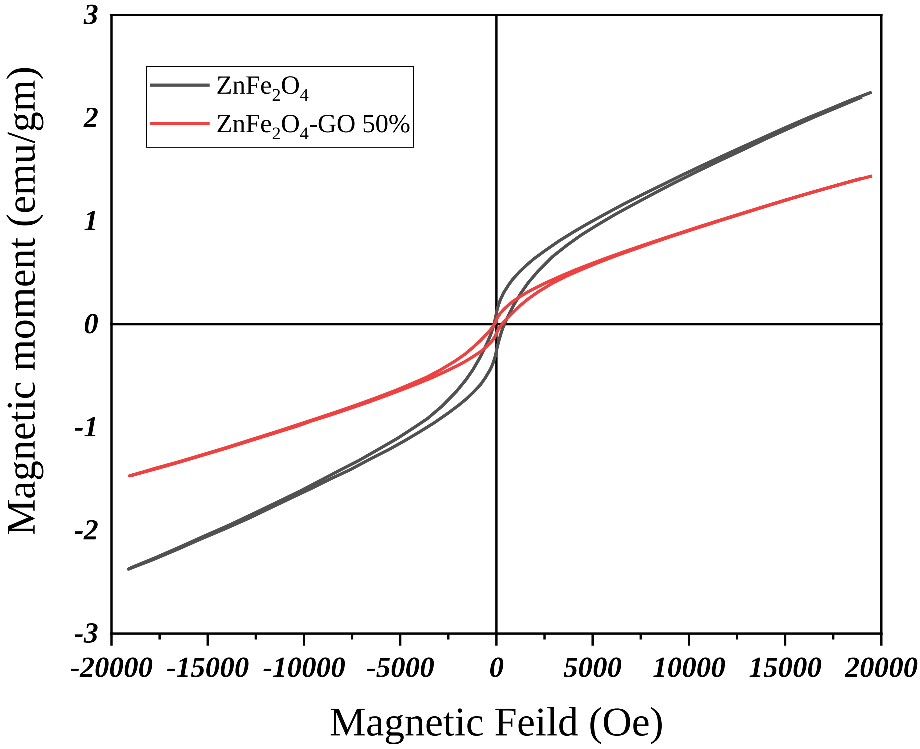

***Fig (5)*:** Magnetization curves obtained by VSM at room temperature.

3.6. Dye Adsorption Study

In this work as in Fig (6), which calibration curve of methyl blue (MB) a cationic dye, was utilized. Table 3 shows the percent absorption vs. different concentration of MB graphs for each dye in 200 mL of dye solutions with concentration (25mg/L). This MB has an exceptionally high removal rate, reaching above 95% in just 30 minutes [52].

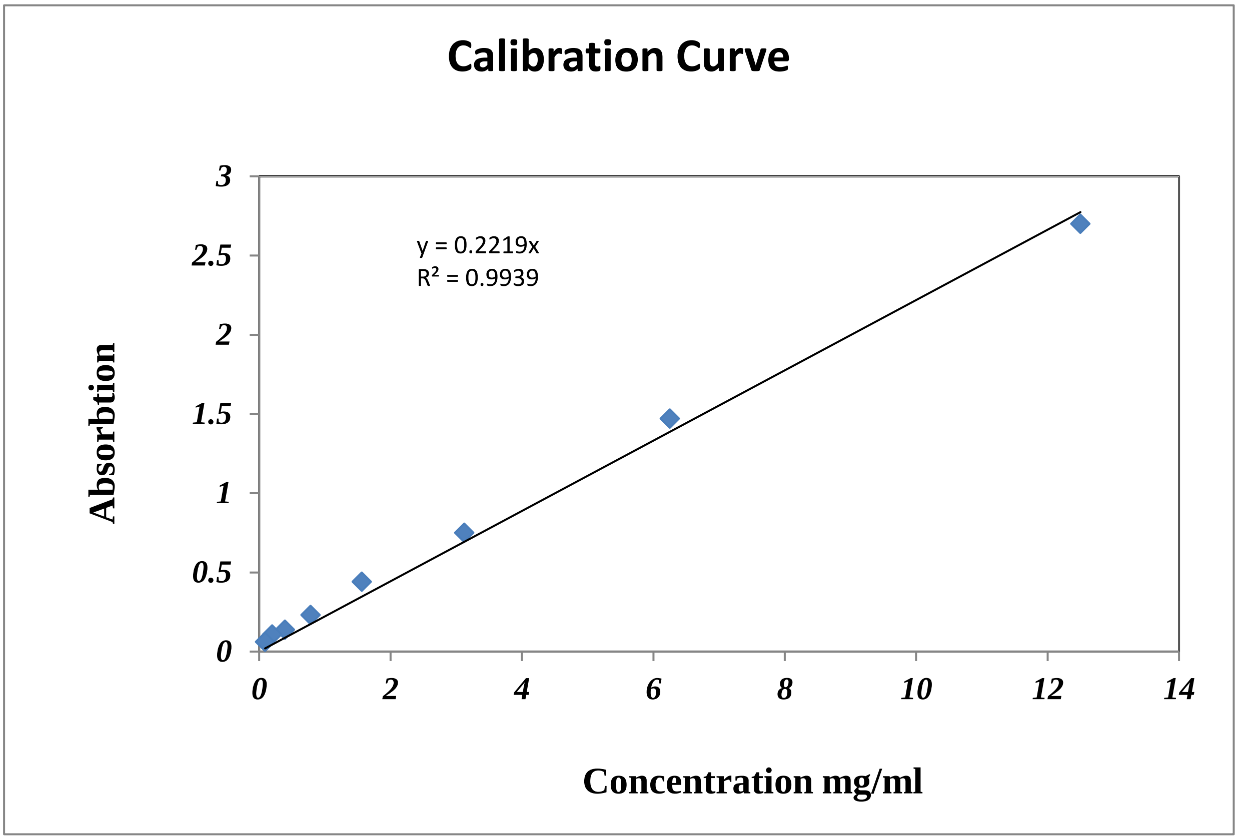

Fig. (6): calibration curve blank

Table (3) The calibration curve of methyl blue (MB) a cationic dye.

Blank 1 (12.5 mg/l) λ (672)

Conc.	Abs
12.5	*2.7*
6.25	*1.47*
3.12	*0.75*
1.56	*0.44*
0.78	*0.23*
0.39	*0.137*
0.195	*0.108*
0.09	*0.06*

3.6.1. Influence of adsorbent dose

3.6.2. Influence of contact time

From Fig (7a), Fig (7b) The adsorption capacity and dye removal efficiency of $ZnFe_2O_4$/Go 50% on MB solution affected by the time, In the first 10 min, the adsorption capacity and removal efficiency of the dye increased rapid with time then the effectiveness of these The $ZnFe_2O_4$/Go compound adsorption The adsorption capacity reach equilibrium gradually noticeably after 30 min [50, 53]. Repulsive forces develop on the adsorbent's surface when the number of these sites gradually diminishes as dye molecules occupy them over time and reach to saturation. As a result, the adsorbent does not readily stick to the material's surface. According to Table 4, $ZnFe_2O_4$/Go has an equilibrium adsorption capacity (qe) of 200 mg L, with the aid of a calibration curve, a UV-visible spectrophotometer was used to quantify the dyes' ultimate absorbance [54].

Qt=(Co-Ce) *V/W (mg/g) .... (2)

Table (4) $ZnFe_3O_4$/Go has an equilibrium adsorption capacity (qe) of 200 mg L, with the aid of a calibration curve, a UV-visible spectrophotometer was used to quantify the dyes' ultimate absorbance.

Contact Time (min)	Abs	Conc.	Removal %	Adsorption Capacity
10	*0.055*	*0.495719*	*98.017125*	*49.00856242*
20	*0.0472*	*0.425417*	*98.298333*	*49.14916629*
30	*0.0461*	*0.415502*	*98.33799*	*49.16899504*
60	*0.044*	*0.396575*	*98.4137*	*49.20684993*
90	*0.0428*	*0.385759*	*98.456963*	*49.2284813*
120	*0.0364*	*0.328076*	*98.687697*	*49.34384858*

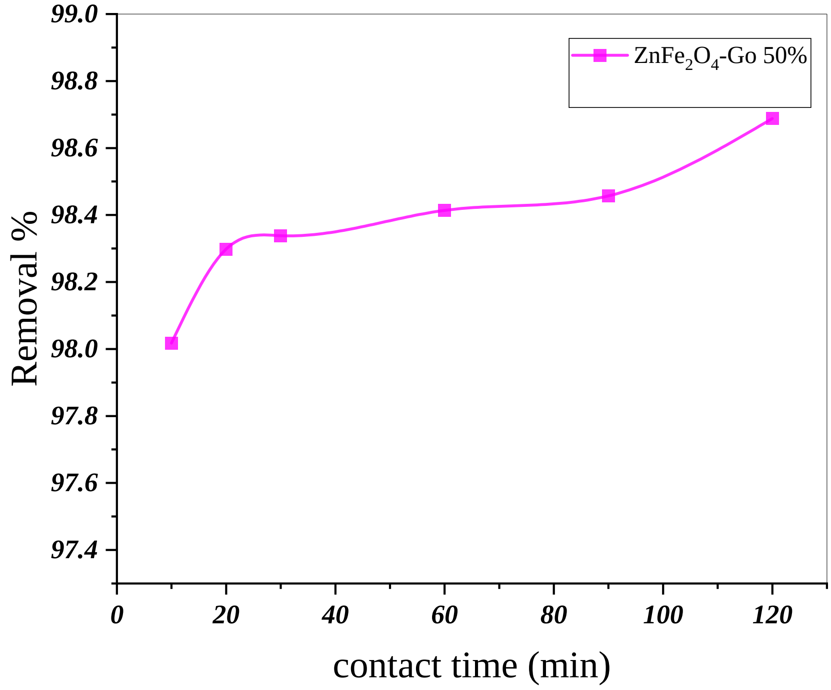

***Fig. (7.a)*:** Effect of the Contact time and the Removal of $ZnFe_2O_4$-GO 50%,

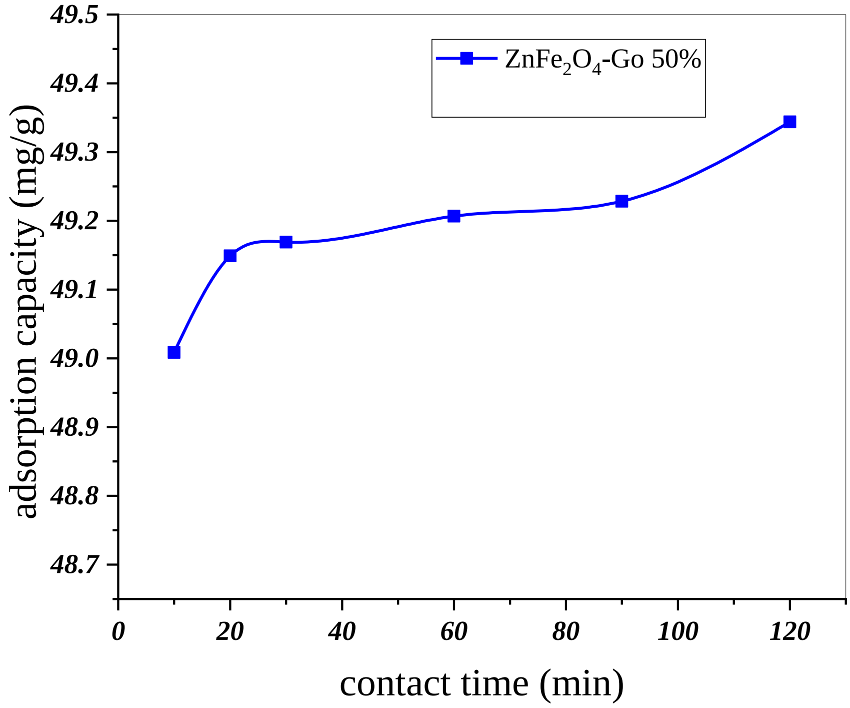

Fig. (7.b): Effect Contact time and the Adsorption Capacity of $ZnFe_2O_4$-GO 50%.

3.6.3. Effect of initial concentration of cationic dye

The initial dye concentration was important since a certain mass of the adsorbent material can only absorb a certain amount of the cationic dye. The results demonstrated that as MB dye content was raised, so was the adsorption capacity. Increasing cationic dye concentration affected the equilibrium concentration of the cationic dye solution, increased the amount of dye absorbed by each unit of ZnFe/GO, and increased the acceleration from the concentration gradient that increased cationic dye's diffusion rate towards ZnFGO [55-56].

Figure 8 illustrated the rate of dye removal in percent against the adsorbate concentrations at certain time of (A) MB, using nanohybrids prepared with initial GO/ $ZnFe_2O_4$ with different concentration. There is just one, and that is to quickly magnetically separate dye-adsorbed composites from an aqueous environment. Contrarily, the $ZnFe_2O_4$ nanoparticles used in this study only had a physical attachment to the GO sheets and were primarily used as magnetic agents to quickly remove GO sheets that had been dye-adsorbed from an aqueous environment. The early yet efficient magnetic separation and the weak attractions between sulfonated GO and $ZnFe_2$O4 nanoparticles are advantages for the hybrid materials described here. In experiments, the amount of dye removal rate obtained using a $ZnFe_2O_4$/Go as produced with various GO concentrations After 30 minutes, GO/ $ZnFe_2O_4$ 50% sample was determined and is shown in Table (5) adsorption with continuous shaking. Utilizing various GO-$ZnFe_2O_4$ nanocomposite doses to remove dye 200 mg/L and 200 mg/L of MB solution were added to a beaker with 12.5mg, 25mg, 50mg, and 100 mg of adsorbent samples. By increasing the adsorbent's Concentrations, the adsorption rate was noticeably increased. It took 30 minutes for 100 mg of adsorbent to reach equilibrium when $ZnFe_2O_4$/GO nanocomposite was present. After reaching equilibrium, the number of adsorbents was increased while MB removal gradually increased [57].

Typically, the microspheres removal efficiency proceeds significantly was affected by the surface area, and as it is a function of the mass of the sorbent, the extent of accessible active sites plays an important role in this context.

Table 5 Adsorption with continuous shaking.

initial conc	Abs	Conc.	Removal %
100 mg	*0.0461*	*0.4155*	*98.338*
50mg	*0.0455*	*0.5666252*	*97.733499*
25mg	*0.0633*	*0.7882939*	*96.846824*
12.5mg	*0.088*	*1.0958904*	*95.616438*

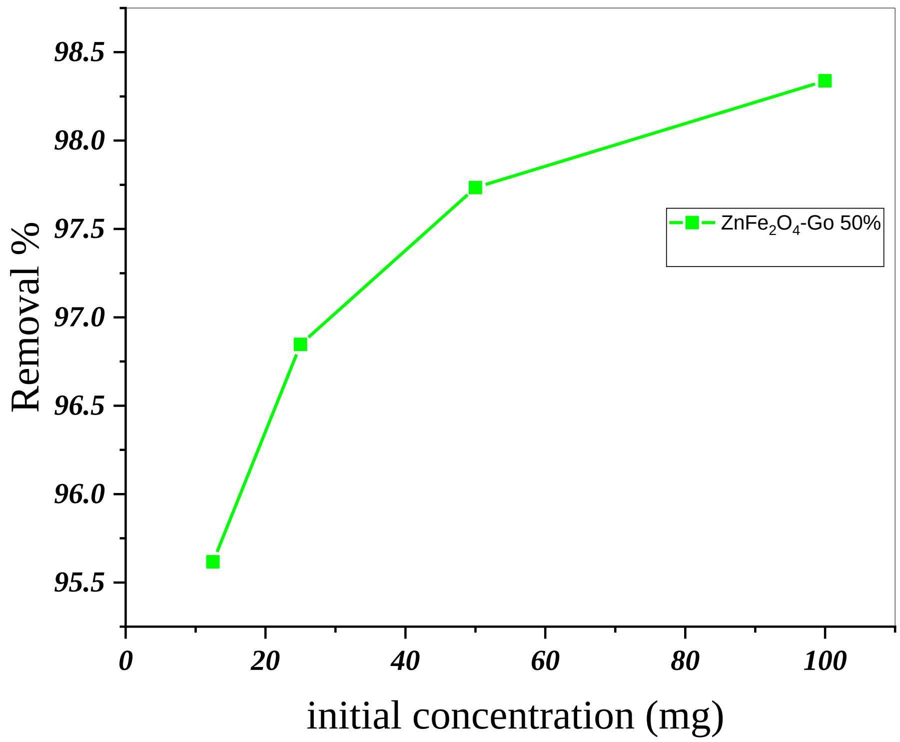

Fig. (8) from different concentration and removal at constant time 30 min.

3.7. Kinetics study of dye removal

The kinetic parameters provide useful information for designing and modeling the adsorption processes as well as for predicting the adsorption rate. In order to explain the adsorption process and kinetics, pseudo-first order and pseudo-second-order models were employed to explore the kinetics of $ZnFe_2O_4$-GO adsorption on the generated nanoparticles. [56.57].

3.7.1. Pseudo-first order model

The linear pseudo-first order kinetic model of Lagergren is given as:

$$\mathbf{Log\ (qe - qt) = Log\ qe - \frac{K1}{2.303}\ t} \quad \text{..................} \quad \textbf{(3)}$$

Where qe and qt are the amounts of MB cation dyes adsorbed onto solution of composite (mg/g) at equilibrium and at time t, respectively, and k1 is the rate constant of pseudo-first order kinetic model (min ^{1}). The straight-line plots of log (qe - qt) against t were used to determine the k1 and correlation coefficient, R_2, as presented in Figs 9 and Table 6. The Pseudo-first order model was set on a hypothesis that the day removal rate is mainly attributed to the free active site number. As presented in Table 6 and fig 9, the obtained results showed that the first-order model can give a realistic judgment of qe for MB removal, as qe (the experimental value) is close to the obtained laboratory data, which indicates that the pseudo-first-order model corroborates conformity to this reaction.

Table (6):

The calculated values of K_1, K_2, qt (theo.), qe (experimental) and R^2 (correlation factor).

Pseudo-first-order kinetic model:

$$\mathbf{Log\ (qe - qt) = Log\ qe - \frac{K1}{2.303}\ t} \quad \text{..................} \quad \textbf{(3)}$$

qe(mg/g)	qt(mg/g)	K_1 (g mg^{-1} min^{-1})	R^2
6.0575	*2.001*	*-0.055*	*0.0977*

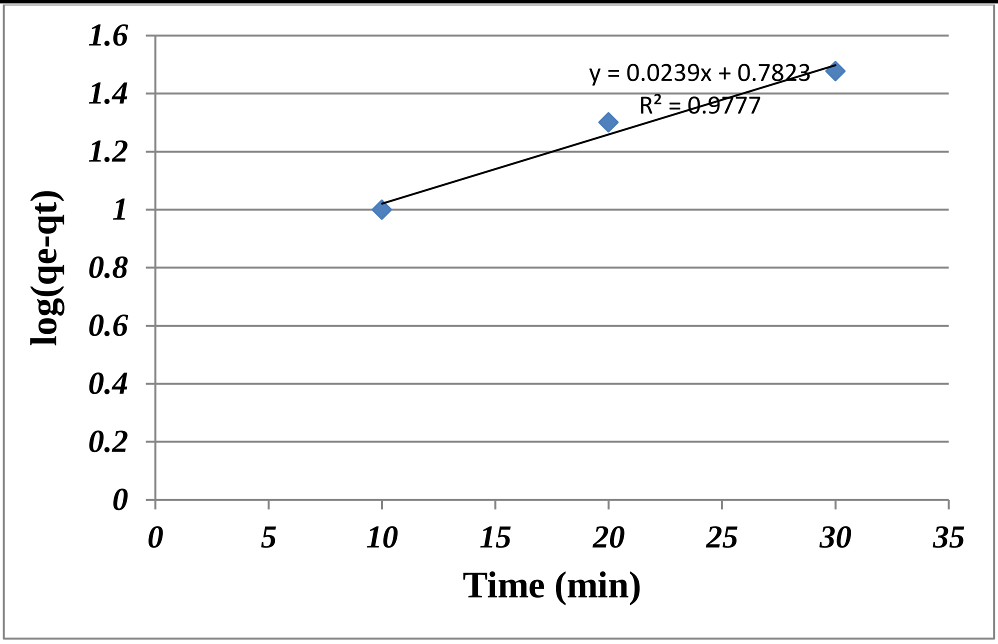

Fig. (9): Pseudo-first order modeling for MB removal using $ZnFe_2O_4$ / GO50% nanocomposite.

3.7.2. Pseudo-second order model

The linear form of the pseudo-second-order equation is given by:

$$\frac{t}{qt} = \frac{1}{K2\ qe^2} + \frac{1}{qe}T \quad .... \quad (4)$$

Where qe and qt are the amounts of of MB cation dyes adsorbed (mg/g) at equilibrium and at time t, and k. is the rate constant of pseudo-second order kinetic model (g/mg.min). The straight-line plots of t/qt against t were used to determine the correlation coefficient, R^2. The pseudo-second order kinetic model was used to determine whether the rate limiting step during the adsorption process was chemisorption. This model was more likely to predict the behavior over the whole range of contact time as shown in fig10 and table 7.

Table (7):

From the y-intercept of the plot, k 2 can be estimated, while q e was determined from the slope.

Pseudo-second-order kinetic model: t/qt = 1/K_2 ·qe2 + 1/qe · T

qe(mg/g)	qt(mg/g)	K_2 (g mg^{-1} min^{-1})	R^2
49.2	*0.726*	*0.00032*	*1*

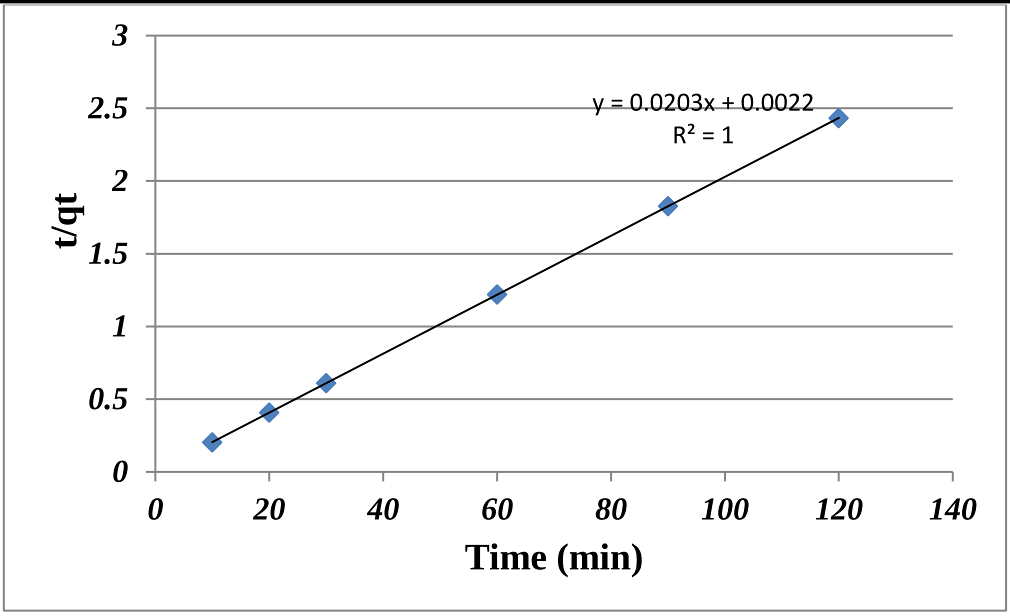

***Fig (10)*:** Pseudo-second order modeling for MB removal using $ZnFe_2O_4$ / GO50% nanocomposite

The related adsorption rate constants are used to determine the reliability of each model, as well as the experimental and calculated data in Figures (9) and (10). For MB adsorption by $ZnFe_2O_4$ / GO50% nanocomposite, the second-order kinetic model's correlation coefficient (R_2 =1) was greater than the first-order kinetic model's (R_2 =0.977) correlation coefficient with the experimental and predicted results. $ZnFe_2O_4$ nanocomposite is being occurred by the adsorption chemistry. In The first phase occurs due to spreading of the adsorbate from the liquor to the adsorbent surface, indicating the faster adsorption for the GO-$ZnFe_2O_4$ nanocomposite with the higher diffusion [58, 59]. The second phase was the adsorbate molecules spread through the adsorbent mi-cropores and in regions, where active sites were difficult to reach by the dye's cation due to the cross-linking between the surface groups.

4. Conclusion

-Spinel nanoferrite (MFe_2O_4) nanoparticles have been synthesized by sol-gel method using citric acide as fulle.

-Graphen Oxide prepared using Hammer technique and the starting raw materials as graphite powder.'

-The average crystallite sizes range from 26.7 -35.1nm.

- FE-TEM was used to examine the interface structure and particle size of samples, which generally had diameters between 25 and 120 nm.

- The $ZnFe_2O_4$ nanoparticle and $ZnFe_2O_4$/GO nanosheet magnetization curves demonstrated that two samples exhibited superparamagnetic characteristics.

- $ZnFe_2O_4$ nanoparticles and $ZnFe_2O_4$/GO 50% had saturation magnetizations (Ms) of 2.7902 and 1.4546 emu/g, respectively.

- All samples may be ideal for low magnetic losses application given the low coercive force values that allow for simple magnetization and demagnetization with small magnetic losses.

-The examination of adsorption efficiency of the end products demonstrated that nanocomposite had a strong adsorption capability and both magnetic characteristics for recovery and proper surface area can nominate the produced nanocomposite as a great adsorbent for water purification. for MB adsorption from $ZnFe_2O_4$/ GO composite which the best composite removal is $ZnFe_2O_4$ /GO which concentration 50% is removal 98.3 % at 30 min and higher removal for MB is 98.68 % at 120 min.

- The related adsorption rate constants are used to determine the reliability of each model, as well as the experimental and calculated data in Figures 3 and 4. For MO adsorption on $ZnFe_2O_4$ / GO50% nanocomposite, the second-order kinetic model's correlation coefficient (R2 =1) was greater than the first-order kinetic model's (R2 =0.977) correlation coefficient with the experimental and predicted results.

- The novelty of this study is accentuated from the saturation magnetization values (Ms) of $ZnFe_2O_4$ nanoparticles and $ZnFe_2O_4$/GO 50% had of 2.7902 and 1.4546.

References

[1] J.Arshad, F.Mohammed ,A.Alzahrani ,S.Munir, U.Younis, M.S.Al-Buriahi, Z.A. Alrowaili, Integration of 2D graphene oxide sheets with MgFe2O4/ZnO heterojunction for improved photocatalytic degradation of organic dyes and benzoic acid, Ceramics International 49: (2023) 18988-19002.

[2] H. Subramanian, H,Santhaseelan, V. T. Dinakaran, V.Devendiran, A. J. Rathinam, A.Mahalingam,S.K.Ramachandran, K. Muthukumar, T.Mathimani, Hydrothermal synthesis of spindle structure copper ferrite-graphene oxide nanocomposites for enhanced photocatalytic dye degradation and in-vitro antibacterial activity, Environmental Research 213: (2023) 116084-116095.

[3] A.S. Eltaweil, A.M. Abdelfatah, M. Hosny, M. Fawzy, Novel biogenic synthesis of a Ag@ Biochar nanocomposite as an antimicrobial agent and photocatalyst for methylene blue degradation, ACS omega **7**: (2022) 8046–8059 .

[4] H. Xue, X. Wang, Q. Xu, F. Dhaouadi, L. Sellaoui, M.K. Seliem, A.B. Lamine, H. Belmabrouk, A. Bajahzar, A. Bonilla-Petriciolet, Adsorption of methylene blue from aqueous solution on activated carbons and composite prepared from an agricultural waste

biomass: A comparative study by experimental and advanced modeling analysis, Chem Eng 430 :((2022) 132801 .

[5] A.s. Eltaweil, E.M.Abd El-Monaem, G.M.El-Subruiti, *et al,* Graphene oxide incorporated cellulose acetate beads for efficient removal of methylene blue dye; isotherms, kinetic, mechanism and co-existing ions studies, *Porous Mater* **30: (2022)** 607–618.

[6] B. Qiu, X.Zhang, S.Xia, T.Sun, Y.Ling, S.Zhou, H.Guang, Y.Chen, Z.Xu, M.Liang.et al. Magnetic graphene oxide/carbon fiber composites with improved interfacial properties and electromagnetic interference shielding performance.,Compos. Part A Appl Sci Manuf 155: (2022) 1-106811

[7] T.Ullah, K.Gul, H.Khan, B.Ara, T.U.H. Zia, Efficient removal of selected fluoroquinolones from the aqueous environment using reduced magnetic graphene oxide/polyaniline composite, Chemosphere 293: (2022) 1-133452.

[8] J.Chen, L.Zhang, H.Li, M.Lu, J.Xie, S.Guan, X.Wang, X.Liu, J.Lu, Preparation and adsorbability of magnetic composites based on cellulose nanofiber/graphene oxide, Colloids Surf. A Physicochem. Eng Asp 639: (2022)1- 128373.

[9] R.Masrour, A. Jabar, Study of magnetic order of domain walls based on zigzag graphene nanoribbons under size effect, Synth Met 273: (2021) 1-116694.

[10] R.Kumar, S. Bhattacharya, P. Sharma, Novel insights into adsorption of heavy metal ions using magnetic graphene composites , Environ Chem Eng 9: (2021) 1- 106212.

[11] M.Adel, M.A Ahmed, A.A.Mohamed, Synthesis and characterization of magnetically separable and recyclable crumbled $MgFe_2 O_4$ /reduced graphene oxide nanoparticles for removal of methylene blue dye from aqueous solutions, Phys Chem Solids149: (2021) 1-109760.

[12] P. Heidari, S.MMasoudpanah, Structural, magnetic and optical properties and photocatalytic activity of magnesium-calcium ferrite powders, Phys Chem Solids 148: (2021) 1-109681.

[13] M.A.S.; Nagaswarupa, H.P.; Kumar, M.R.A.; Ravikumar, C.R.; Kusuma, K.B. Sonochemical synthesis of MnFe2O4nanoparticles and their electrochemical and photocatalytic properties, Phys Chem Solids 148: (2021) 1-109661.

[14] A.M. Abdelfatah, M. Fawzy, A.S. Eltaweil, M.E. El-Khouly, Green synthesis of nano-zero-valent iron using ricinus communis seeds extract: characterization and application in the treatment of methylene blue-polluted water,ACS omega 6: (2021) 25397–25411 .

[15] A.S. Eltaweil, E.M. Abd El-Monaem, A.M. Omer, R.E. Khalifa, M.M. Abd El-Latif, G.M. El-Subruiti, Efficient removal of toxic methylene blue (MB) dye from aqueous solution using a metal-organic framework (MOF) MIL-101 (Fe): isotherms, kinetics, and thermodynamic studies, Desalin. Water Treat. 189: (2020) 395–407.

[16] E.H.El-Ghazzawy, Effect of heat treatment on structural, magnetic, elastic and optical properties of the co-precipitated $Co_{0.4}Sr_{0.6}Fe_2O_4$, Magn Magn Mater 497: (2020) 1-166017.

[17] M.S. Amulya, H.Nagaswarupa, M.A.Kumar, C.Ravikumar, K.Kusuma, Sonochemical synthesis of MnFe2O4 nanoparticles and their electrochemical and photocatalytic properties, Phys Chem Solids148: (2020) 1-109661

[18] A.H. Jawad, A.S. Abdulhameed, A. Reghioua, Z.M. Yaseen, Zwitterion composite chitosan-epichlorohydrin/zeolite for adsorption of methylene blue and reactive red 120 dyes. Int, Biol Macromol 163: (2020) 756–765.

[19] J.Chen, M.Ming, C.Xu, J.Wu, Y.Wang, T.Sun, Y.Zhang, G.Fan , Nanosized iron oxide uniformly distributed on 3D carbon nanosheets: Efficient adsorbent for methylene blue ,Appl Sci 9: (2019) 1-2898.

[20] A.R,Abbasian, M.S.Afarani, One-step solution combustion synthesis and characterization of ZnFe2O4 and ZnFe1.6O4 nanoparticles, Appln Phys A Mater Sci Process 125: (2019) 1- 721.

[21] J. Yang, B. Hou, J. Wang, B. Tian, J. Bi, X. li, X. Huang. Nanomaterials for the removal of heavy metals from wastewater, Nanomaterials 9(3): (2019) 1-424.

[22] R.Nivetha, A.N. Grace, Manganese and zinc ferrite based graphene nanocomposites for electrochemical hydrogen evolution reaction, Journal of Alloys and Compounds 796: (2019)185–195.

[23] Y. Miyah, A. Lahrichi, M. Idrissi, A. Khalil, and F. Zerrouq , Adsorption of methylene blue dye from aqueous solutions onto walnut shells powder, Surfaces and Interfaces 11: (2018) 74-81.

[24] M. A. Lelifajri, S. Nawi, Sabar, Supriatno, and W. I. Nawawi, Preparation of immobilized activated carbon-polyvinyl alcohol composite for the adsorptive removal of 2,4-dichlorophenoxyacetic acid, Water Process Engineering 25: (2018) 269-277.

[25] E. Yarahmadi, K. Didehban, M. Shabanian, M. R. Saeb, High-Performance Starch-Modified Graphene Oxide/Epoxy Nanocomposite Coatings: A glimpse at Cure Kinetics and Fracture Behavior, Prog. Color Colorants Coat 11: (2018) 55-62.

[26] N. Ambikeswari, S. Manivannan, ,Superior magnetodielectric properties of room temperature synthesized superparamagnetic cobalt ferrite—Graphene oxide composite, Alloys Compound 763: (2018) 711–718.

[27] R. Shu,G. Zhang,J.Zhang,X.Wang,M.Wang,.Y. Gan, J.Shi, Fabrication of reduced graphene oxide/multi-walled carbon nanotubes/zinc ferrite hybrid composites as high-performance microwave absorbers, Alloys Compound 736: (2018) 1–11.

[28] L.Zheng, L.Guan, G.Yang, S.Chen, H.Zheng, One-pot synthesis of $CoFe_2$ O /rGO hybrid hydrogels with 3D networks for high capacity electrochemical energy storage devices, RSC Adv 8:((2018) 607–8614.

[29] R. Masrour, A.Jabar, Size and diluted magnetic properties of diamond shaped graphene quantum dots: Monte Carlo study, Phys A Stat Mech Appl 497: (2018) 211–217.

[30] S. Martinez-Vargas, A. I. Martínez, E. E. HernándezBeteta, O. F. Mijangos-Ricardez, V. VázquezHipólito, C. Patino-Carachure, J. López Luna. As (III) and As (V) adsorption on manganese ferrite nanoparticles, Mol Struct 1154: (2018) 524-534.

[31] R.E. El Shater, E.H.El-Ghazzawy, M.K.El-Nimr, Study of the sintering temperature and the sintering time period effects on the structural and magnetic properties of M-type hexaferrite $BaFe_{12}O_{19}$,Alloys Compound 739: (2018) 327–334.

[32] P. T. L. Huong, N. Tu, H. Lan, N. V. Quy, P. A. Tuan, N. X. Ding, V. N. Phan, Le A. Tuan, Functional manganese ferrite/graphene oxide nanocomposites: effects of graphene oxide on the adsorption mechanisms of organic MB dye and inorganic As(V) ions from aqueous solution, RSC Adv 8(22): (2018) 12376-12389.

[33] J.Sanchez-Marcos, E.Mazario, J.A.Rodriguez-Velamazan, E.Salas, P.Herrasti, N.Menendez, Cation distribution of cobalt ferrite electrosynthesized nanoparticles A methodological comparison, Alloys Compound 739: (2018) 909–917.

[34] L.P. Lingamdinne, J.-S. Choi, J.-K. Yang, Y.-Y. Chang, J.R. Koduru, J. Singh, Adsorptive removal of selected anionic and cationic dyes by using graphitic carbon material prepared from edible sugar: A study of kinetics and isotherms, Acta Chim Slov **65**: (2018) 599–610

[35] X. Jiang, H. Xia, L. Zhang, J. Peng, S. Cheng, J. Shu, C. Li, Q. Zhang, Ultrasound and microwave-assisted synthesis of copper-activated carbon and application to organic dyes removal. Powder Technol **338**: (2018) 857–868.

[36] Z.J. Li, et al. Enhanced photocatalytic removal of uranium(VI) from aqueous solution by magnetic TiO2/Fe3O4 and its graphene composite, Environ Sci Technol 51: (2017) 5666–5674.

[37] L.P. Lingamdinne, et al. Preparation and characterization of porous reduced graphene oxide based inverse spinel nickel ferrite nanocomposite for adsorption removal of radionuclides, Hazard Mater 326: (2017) 145-156 .

[38] N. H. Hieu, T. B. Kiet, N. H. Kiem, N. T. M. Huyen. Removal of Cd (II) from water by using graphene oxide-Mn2O4 magnetic nanohybrids, Journal of Science and Technology 55(1B):(2017) 109-121.

[39] R.Masrour, A.Jabar, Magnetic properties of bilayer graphene armchair nanoribbons: A Monte Carlo study, Magn. Mater 426: (2017) 225–229.

[40] F. Meng, M.Yang, L.Zhao, Y.Zhang, X.Shang, P. Jin, W.Zhang, A comparative study of the structural, magnetic and electrochemical properties of Al^{3+} and Cu^{2+} substituted Ni Zn ferrite/reduced graphene oxide nanocomposites, Ceramics International 43: (2017) 15959-15964

[41] L.Dong, J.Yang, M.Chhowalla ,KP. Loh , Synthesis and reduction of large sized graphene oxide sheets, Chemical Society Reviews 46: (2017) 7306–16.

[42] B.Bashir, W.Shaheen, M.Asghar, M.F.Warsi, M.A.Khan, S.Haider, I.Shakir, M.Shahid,Copper doped manganese ferrites nanoparticles anchored on graphene nano-sheets for high performance energy storage applications, Alloys Compound 695: (2017) 881–887.

[43]] H.V. Kumar, Y.S. Huang, S.P. Ward, D. H. Adamson , Altering and investigating the surfactant properties of graphene oxide,Colloid and Interface Science 493 :(2017) 365-370.

[44] S.Supriya, S.Kumar, M.Kar, CFO-graphene nano composite for high performance electrode material. Mater, Today Proc 4: (2017) 5651–5656.

[45] R. Liu, Y. Cheng, Y. Li, Q. Zhang, B. Jia, D. Wang, R. Fan, Adsorption Kinetics and Adsorption Isotherms of Bovin Serum Albumin (BSA) onto Magnetic $ZnFe_2O_4$ Nanoparticles Nanoscience and Nanotechnology 17:(2017) 2899-2905.

[46] D. Robati, M. Rajabi, O.Moradi, F. Najafi, I.Tyagi, S.Agarwal, V.KGupta, Kinetics and thermodynamics of malachite green dye adsorption from aqueous solutions on graphene oxide and reduced graphene oxide, Mol Liq 214 : (2016) 259–263.

[47] N. U. Yamaguchi, R. Bergamasco and S. Hamoudi, Magnetic $MnFe_2O_4$- graphene hybrid composite for efficient removal of glyphosate from water, Chemical Engineering 295: (2016) 391–402.

[48] N,Pan, et al. Preparation of graphene oxide-manganese dioxide for highly efcient adsorption and separation of T(IV)/U(VI), Hazard Mater 309: (2016) 107-115 .

[49] D.Zhao, et al. Facile preparation of amino functionalized graphene oxide decorated with Fe3O4 nanoparticles for the adsorption of Cr (VI), Appl Surf Sci 384: (2016) 1-9.

[50] N.Mubarak, J.Sahu, E. Abdullah, N. Jayakumar, Plam oil empty fruit bunch based magnetic biochar composite comparison for synthesis by microwave-assisted and conventional heating, Anal Appl Pyrolysis 120: (2016) 521−528.

[51] X.Wu, Q.Wang, W.Zhang, Y.Wang, W.Chen, Nano nickel oxide coated graphene/polyaniline composite film with high electrochemical performance for flexible supercapacitor ,Electrochim. Acta 211: (2016) 1066–1075.

[52] H.Yang, T.Ye, Y. Lin,J. Zhu, F.Wang, F,Microwave absorbing properties of the ferrite composites based on graphene, Alloys Compound 683: (2016) 567–574.

[53] S. Lin, L.Dong , J.Zhang , H.Lu , Room-temperature intercalation and ∼1000- fold chemical expansion for scalable preparation of high-quality graphene, Chemistry of Materials 28: (2016) 2138–2146.

[54]Y.Lin, X.Liu, H.Yang, F.Wang, C.Liu, Synthesis and characterization of graphene/0.8$BaFe_{12}O_{19}$/0.2Y_3 Fe_5 O_{12} nanocomposite, Alloys Compound 683: (2016)559–566.

[55] M. Khazaei, S. Nasseri, M. R. Ganjali, M. Khoobi, R. Nabizadeh, A. H. Mahvi, S. Nazmara, E. Gholibegloo,Response surface modeling of lead (II) removal by graphene oxide-Fe_3O_4 nanocomposite using central composite design, Environmental Health Science and Engineering 2: (2016) 1-14.

[56] N. X. Dinh, D. T. Chi, N. T. Lan, H. Lan, H. V. Tuan, N. V. Quy, V. N. Phan, T. Q. Huy and A. T. Le, Water-dispersible silver nanoparticles-decorated carbon nanomaterials: synthesis and enhanced antibacterial activity, Appl Phys A 119: (2015) 85–95.

[57] Y. Liu, C. Luo, G. Cui, S. Yan. Synthesis of manganese dioxide/iron oxide/graphene oxide magnetic nanocomposites for hexavalent chromium removal, RSC Adv 5: (2015) 54156-54164.

[58] R. Rezaee, S. Nasseri, A. H. Mahvi, R. Nabizadeh, S. A. Mousavi, A. Rashidi, A. Jafari, S. Nazmara, Fabrication and characterization of a polysulfone graphene oxide nanocomposite membrane for arsenate rejection from water, Environmental Health Science and Engineering 61: (2015) 1-13.

[59] A. Meidanchi, O. Akhavan, Superparamagnetic zinc ferrite spinel–graphene nanostructures for fast wastewater purification, Carbon 69: (2014) 230-238.

الملخص العربى

تلوث المياه ومعالجته باستخدام المركبات النانوية مع أكسيد الجرافين

(Zn^{+2}-GO 50 %) لمختلف الأصباغ والمعادن الثقيلة باستخدام طريقه sol -gel

(أ)رحاب عطيه ، (أ) نجوي عكاشه ، (ب) علي عزب ، (ج) احمد بكر

(أ). قسم الفيزياء ، كلية البنات للاداب والعلوم والتربيه ، جامعة عين شمس ، القاهرة ، مصر

(ب) قسم فيزياء الجوامد ، معهد بحوث الفيزياء ، المركز القومي للبحوث ، 33 شارع البحوث ، الدقي ، الجيزة 12622 ، مصر.

(ج) قسم الطيف، معهد البحوث الفيزيقية، المركز القومى للبحوث،33 شارع البحوث ، الدقي ، الجيزة 12622 ، مصر.

تناول البحث المعروض انه تم تصنيع جسيمات نانوية فريتيه (MFe_2O_4) بطريقة sol-gel باستخدام حامض الستريك كمادة محفزه .

بينما تم تحضير أكسيد الجرافين باستخدام تقنية المطرقة والمواد الأولية ا كمسحوق الجرافيت. علاوه علي ذلك تم اكتشاف انشاء جسيمات نانومتريه مطليه باكسيد الجرافين(MFe_2O_4 -GO(M = Zn.العنصر المعدني). بالاضافه الي ذلك يتسبب أكسيد الجرافين (GO) أيضًا في احتواء المركب على جسيمات نانوية ذات حجم أبعاد أصغر(<10 نانومتر). كما ان وجد بأن المركب يتميز $ZnFe_2O_4$ بالعديد من التقنيات الفيزيائية والكيميائية، مثل حيود الأشعة السينية (XRD) حيث يتراوح متوسط أحجام البلورات من 26.7 إلى 35.1 نانومتر . وقد تم تم فحص التشكل السطحي وحجم الجسيمات للعينات باستخدام FE-TEM بأقطار تتراوح في كثير من الأحيان من 25 إلى 120 نانومتر. وتم قياس الخواص المغناطيسيه لهذا المركب كقياس Ms ,Hc للمركب، حيث وجد في منحنيات المغنطة من انخفاض قيمه Hc مما يشير إلى أن عيناتنا عبارة عن مادة مغناطيسية ناعمه . كما وجد قيم مختلفه لمنطقه التشبع وذلك لتواجد مركب اكسيد الجرافين التي ادت الي تقليل قيمه مغنطة التشبع (Ms) ، واثبتت النتايج ذلك Ms $ZnFe_2O_4$ = 2.79 emu ولكن Ms للعينه $ZnFe_2O_4$- Go 50 % بتساوي 1.4546 emu. وفي النهايه وفقا للنتايج اثبت ان المركب الذي تم تحضيره MFe2O4 يتميز بمسامية ومساحة سطحية عالية بالإضافة إلى مغنطة تشبع كبيرة ، مما يجعله منافسًا واعدًا لعدد من التطبيقات .